Supplementary Information for: "One- and two-dimensional nuclear magnetic resonance spectroscopy with a diamond quantum sensor"

J. M. Boss[1], K. Chang[1], J. Armijo[2], K. Cujia[1], T. Rosskopf[1], J. R. Maze[2], and C. L. Degen[1]

[1]*Department of Physics, ETH Zurich, Otto Stern Weg 1, 8093 Zurich, Switzerland*

[2]*Departmento de Física, Pontificia Universidad Católica de Chile, Santiago 7820436, Chile*

I. THE ROTATING FRAME OF THE NV CENTER

The goal of this section is to clarify our notation and shortly derive Eq. (3) in the main text, which is the Hamiltonian describing the two spin system of the NV center and the ^{13}C nuclear spin in a rotating frame of the NV center resonant with the $m_s = 0 \leftrightarrow m_s = -1$ spin transition.

We start with the Hamiltonian for the NV center (spin 1), ^{13}C nuclear spin (spin $\frac{1}{2}$) and their hyperfine interaction:

$$\hat{H} = D_{gs}\hat{S}_z^2 + \gamma_\mathrm{e}\vec{S}\cdot\vec{B} + \vec{S}\mathbf{A}\vec{I} - \gamma_\mathrm{n}\vec{I}\cdot\vec{B}, \tag{S1}$$

where $D_{gs} = 2.8\,\mathrm{GHz}$ is the zero-field spitting and $\mathbf{A}$ is the hyperfine tensor. If we assume the external B-field to point along the positive z-axis we get the slightly simpler Hamiltonian

$$\hat{H} = \left(D_{gs}\hat{S}_z^2 + \gamma_\mathrm{e}B_0\hat{S}_z\right) + \vec{S}\mathbf{A}\vec{I} + \gamma_\mathrm{n}B_0\hat{I}_z. \tag{S2}$$

From the term $\left(D_{gs}\hat{S}_z^2 + \gamma_\mathrm{e}B_0\hat{S}_z\right)$ one sees that for non-zero external B-field there are two resonances, hence two choices for a rotating frame $D_{gs} \pm \gamma_\mathrm{e}B_0$. As we used the $m_s = 0 \leftrightarrow m_s = -1$ spin transition for our experiment, we transform in a rotating frame resonant with this transition. The rotation is given by $e^{-it\omega_\mathrm{rot}\hat{S}_z}$ with $\omega_\mathrm{rot} = (D_{gs} - \gamma_\mathrm{e}B_0)$ and the Hamiltonian in the rotating frame takes the form

$$\hat{H}_\mathrm{rot} = D_{gs}\left(\hat{S}_z^2 + \hat{S}_z\right) + e^{-it\omega_\mathrm{rot}\hat{S}_z}\vec{S}\mathbf{A}\vec{I}e^{it\omega_\mathrm{rot}\hat{S}_z} + \gamma_\mathrm{n}B_0\hat{I}_z. \tag{S3}$$

In the rotating wave approximation, where the coupling between the nuclear spin and the NV center is far slower than the rotating frame frequency ω_{rot}, we drop all components of the hyperfine tensor that do not commute with $\hat{S}_z$.

$$\hat{H}_{\mathrm{rot}} = D_{gs}\left(\hat{S}_z^2 + \hat{S}_z\right) + a_{||}\hat{S}_z\hat{I}_z + a_{\perp}\hat{S}_z\hat{I}_x - \gamma_{\mathrm{n}}B_0\hat{I}_z \tag{S4}$$

We see, that the $m_s = 1$ state is far detuned form our rotating frame and is therefore not affected by the pulse sequences which we apply during our experiment. Therefore, we will restrict ourselves to the $\{m_s = 0,\ m_s = -1\}$ subspace from now on. To make this more obvious, we change our notation, such that $S_{x,y,z}$ are spin $\frac{1}{2}$ operators. The Hamiltonian from Eq. (S4) becomes

$$\hat{H} = \omega_0\hat{I}_z + a_{||}\left(\hat{S}_z + \hat{S}_e\right)\hat{I}_z + a_{\perp}\left(\hat{S}_z + \hat{S}_e\right)\hat{I}_x, \tag{S5}$$

where $\hat{S}_z = \frac{1}{2}\left\{|1\rangle\langle 1| - |0\rangle\langle 0|\right\}$ and $\hat{S}_e = \frac{1}{2}\left\{|0\rangle\langle 0| + |1\rangle\langle 1|\right\}$ and $\omega_0 = -\gamma_{\mathrm{n}}B_0$ is the Larmor frequency of the nuclear spin. Please note, that $|1\rangle$ denotes the $m_s = -1$ state of the NV center.

The advantage of using spin $\frac{1}{2}$ operators to describe the NV centers Hamiltonian is most apparent when using product operators to compute measurement outcomes, as it is done in the main manuscript.

II. DEVIATION BETWEEN MEASURED HYPERFINE PARAMETERS $a'_{||}$, $a'_{\perp}$ AND EXACT HYPERFINE PARAMETERS $a_{||}$ AND $a_{\perp}$

One goal of our experiments is to precisely determine the hyperfine parameters. We have used two pulse protocols to determine $a_{||}$ and $a_{\perp}$: In the first protocol no pulses are applied during the free precession period. In the second protocol a CP-type sequence of electronic π pulses is applied to generate a nuclear Rabi rotation. For small hyperfine coupling, where $a_{\perp}, a_{||} \ll \omega_0$, the free precession Hamiltonians for the two pulse protocols are (see Fig. 1c):

$$\hat{H}^{(2)}_{\mathrm{free}} = \omega_0\hat{I}_z + a_{||}\left(\hat{S}_z + \hat{S}_e\right)\hat{I}_z \tag{S6}$$

$$\hat{H}^{(3)}_{\mathrm{free}} = \frac{a_{\perp}}{\pi}\left(2\hat{S}_z\right)\hat{I}_x \tag{S7}$$

Thus, the two protocols produce signals with frequencies ω_0 and $\omega_0 + a_{||}$ [Eq. (S6)] as well as $a_{\perp}/\pi$ [Eq. (S7)].

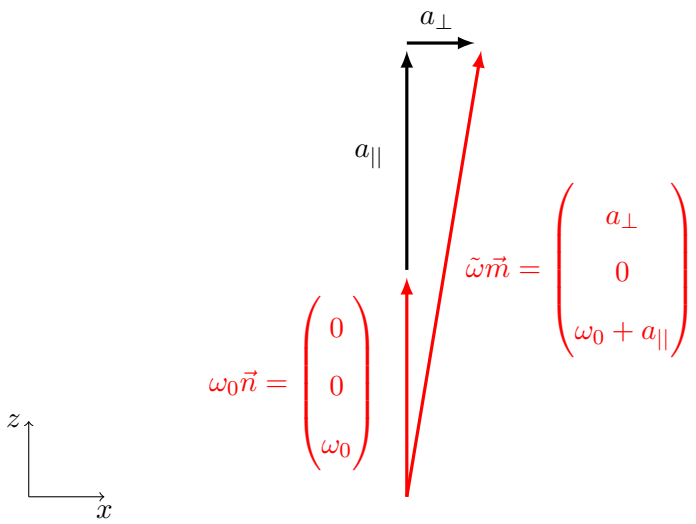

FIG. S1: Sketch depicting the rotation axes of the nuclear spin with and without additional hyperfine field. $\vec{n}$ and $\vec{m}$ are the normalized unit length rotation axes.

These two relations are exact only in the limit of vanishing hyperfine coupling, where $a_{||}/\omega_0 \to 0$ and $a_\perp/\omega_0 \to 0$. For a finite hyperfine coupling, the measured rotation frequencies deviate from these values because the $a_\perp$ leads to a tilt of the nuclear quantization axis. We in the following calculate the exact hyperfine parameters $a_{||}$ and $a_\perp$ compare them with the measured parameters $a'_{||}$ and $a'_\perp$.

A. Calculation of hyperfine parameters form measured frequencies

In the first protocol no pulses are applied during the free precession period. Conditional on the NV spin state the nuclear spin evolves under one of the following Hamiltonians:

$$\hat{h}_0 = \omega_0 \hat{I}_z \quad \text{and} \tag{S8}$$

$$\hat{h}_1 = (\omega_0 + a_{||})\hat{I}_z + a_\perp \hat{I}_x \tag{S9}$$

Here, $\hat{h}_0$ denotes the nuclear Hamiltonian for the NV center being in the $|0\rangle$ state and $\hat{h}_1$ denotes the nuclear Hamiltonian for the NV center being in the $|1\rangle$ state.

Evolution under $\hat{h}_0$ and $\hat{h}_1$ leads to rotations with the frequencies

$$\omega_0 \qquad \text{under } \hat{h}_0, \tag{S10}$$

$$\tilde{\omega} = \sqrt{(\omega_0 + a_{||})^2 + a_\perp^2} \qquad \text{under } \hat{h}_1. \tag{S11}$$

Thus, the frequency that we measure during the free precession are ω_0 and $\tilde{\omega}$. In the second protocol we apply a CP sequence during the free precession time, with basic building block of $(\tau/2 - \pi - \tau - \pi - \tau/2)$, where π denotes π pulses and τ is the interpulse delay. This leads to an I_x rotation of the nuclear spin as described in the Supplemental Material of Taminiau et al. [S1]. We interpret the measured modulation as a Rabi oscillation with frequency ω_1. The average phase 2ϕ picked up by the nuclear spin during the time 2τ is given by

$$\cos(2\phi) = \cos\left(\omega_0 \frac{\tau}{2}\right) \cos\left(\tilde{\omega} \frac{\tau}{2}\right) - \frac{\omega_0 + a_{||}}{\tilde{\omega}} \sin\left(\omega_0 \frac{\tau}{2}\right) \sin\left(\tilde{\omega} \frac{\tau}{2}\right), \tag{S12}$$

where

$$2\phi = \pi - \omega_1 \tau. \tag{S13}$$

Please note that the phase 2ϕ is defined by the rotation

$$\exp\left(i2\phi(\vec{k} \cdot \vec{\hat{\sigma}})\right) = \mathbf{1}\cos(2\phi) + i(\vec{n} \cdot \hat{\vec{\sigma}})\sin(2\phi), \tag{S14}$$

where $\vec{k}$ is a unit length rotation axis and $\vec{\hat{\sigma}}$ is the vector of Pauli matrices. When $2\phi = \pi$, as it is the case for a vanishing transverse hyperfine interaction, the above rotation equals minus the identity. The measured Rabi phase is the deviation from $2\phi = \pi$ during the sequence time of 2τ.

We can solve Eq. (S12) for $a_{||}$ and then use Eq. (S11) to find $a_\perp$.

$$a_{||} = \tilde{\omega}\left(\frac{\cos\left(\tilde{\omega}\frac{\tau}{2}\right)\cos\left(\omega_0\frac{\tau}{2}\right) - \cos(2\phi)}{\sin\left(\tilde{\omega}\frac{\tau}{2}\right)\sin\left(\omega_0\frac{\tau}{2}\right)}\right) - \omega_0 \tag{S15}$$

$$a_\perp = \sqrt{\tilde{\omega}^2 - \left(\omega_0 + a_{||}\right)^2} \tag{S16}$$

We have performed numerical simulations based on the density matrix to verify that Eq. (S15) and Eq. (S16) are exact.

III. FITTING OF SIGNAL FREQUENCIES

Reported values for ω_0, $a_{||}$ and $a_\perp$ were obtained by fitting the time signals of the free precession, and then calculating parameters from the fitted frequencies.

A. Fitting of measured signals

The free precession under the Hamiltonian $\hat{H}^{(2)}_{\text{free}}$ results in a signal that has two frequency components. As discussed in the main text this is due to the NV center being in a superposition state during the free precession. To fit the data shown in Fig. S2 (a) we used the following model function:

$$s^{(2)}(t) = A\cos(2\pi\nu_1 t + \alpha_1) + B\cos(2\pi\nu_2 t + \alpha_2) + C\,. \tag{S17}$$

The two reported frequencies (see Table I) were then up-shifted by 8 and 24 times the sampling frequency because the data was 8-fold and 24-fold under sampled. Since the time signal did not show significant amplitude decay we omitted the decay term from the model.

The signal resulting from the free precession under Hamiltonian $\hat{H}^{(3)}_{\text{free}}$ was not under sampled and had only one frequency component. However, due to imperfections in the CP sequence, the signal decayed somewhat faster than expected from T_1. The model function used was:

$$s^{(3)}(t) = A\cos(2\pi\nu_3 t + \alpha)\exp(-t/T_{1,\text{CP}}) + C\,, \tag{S18}$$

where $T_{1,\text{CP}}$ is the longitudinal decay time for the NV center under the CP sequence.

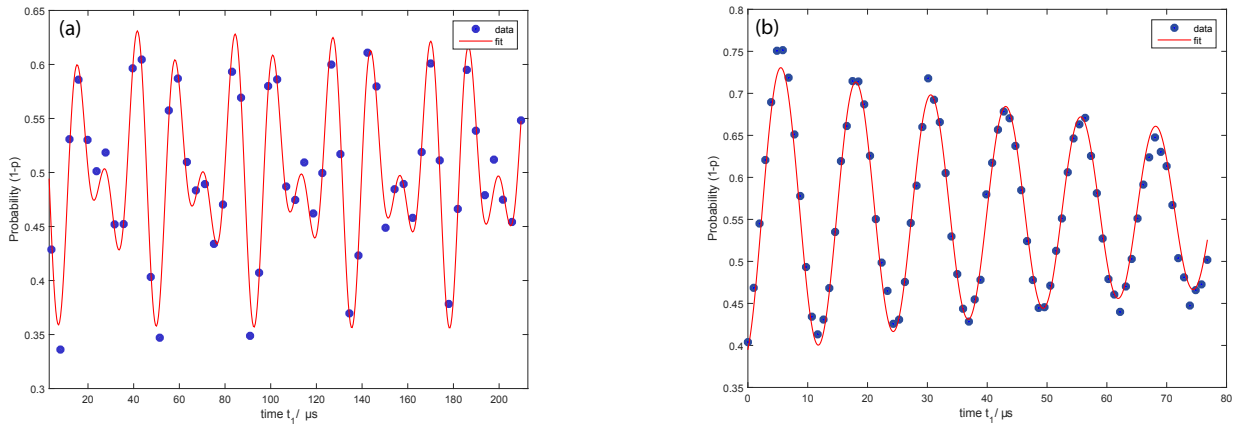

FIG. S2: Precision measurement of $\omega_{0,n}$, $a_{||}$ and $a_{\perp}$. (a) Free precession signal under Hamiltonian $\hat{H}^{(2)}_{\text{free}}$ with 8-fold and 24-fold under sampling for $\omega_{0,n}$ and $a_{||}$, respectively. (b) Free precession signal under Hamiltonian $\hat{H}^{(3)}_{\text{free}}$.

Measurement	NMR constants	
$\nu_1 = 2.09320(11)$ MHz	$\omega_0/2\pi = 2.09320(11)$ MHz	
$\nu_2 = 6.11671(11)$ MHz	$a'_{\|\|}/2\pi = 4.02350(16)$ MHz	$a_{\|\|}/2\pi = 4.00195(30)$ MHz
$\nu_3 = 0.07980(13)$ MHz	$a'_{\perp}/2\pi = 0.25070(41)$ MHz	$a_{\perp}/2\pi = 0.5132(17)$ MHz

TABLE I: Measured frequencies $\nu_{1..3}$, Larmor frequency ω_0, effective hyperfine constants $a'_{||}$, $a'_{\perp}$ and exact hyperfine constants $a_{||}$, $a_{\perp}$ for the ^{13}C nuclear spin from Fig. 3 and Fig. 4.

B. Estimation of hyperfine parameters

We calculated $a'_{||}$ and $a'_{\perp}$ as well as $a_{||}$ and $a_{\perp}$ from the fitted frequencies. The results are summarized in Table I. The final values were then confirmed by a density matrix simulation.

1. *Calculation of $a'_{||}$ and $a'_{\perp}$*

The constants ω_0, $a'_{||}$ and $a'_{\perp}$ in the limit of vanishing hyperfine coupling are:

$$\omega_0 = 2\pi\ \nu_1 \tag{S19}$$

$$a'_{||} = 2\pi\ (\nu_2 - \nu_1) \tag{S20}$$

$$a'_{\perp} = 2\pi\ \pi\nu_3 \tag{S21}$$

These values are reported in the second column of Table I.

2. *Calculation of $a_{||}$ and $a_{\perp}$*

To account for the strong hyperfine coupling we used Eq. (S15) and Eq. (S16) to calculate $a_{||}$ and $a_{\perp}$. The rotational phase under the CP sequence is given by $2\phi = \pi - 2\pi\nu_3\tau$. The interpulse delay for this particular measurement was $\tau = 121.5\,\text{ns}$.

$$a_{||} = 2\pi\nu_2 \left(\frac{\cos\left(2\pi\nu_2\frac{\tau}{2}\right)\cos\left(2\pi\nu_1\frac{\tau}{2}\right) - \cos(\pi - 2\pi\nu_3\tau)}{\sin\left(2\pi\nu_2\frac{\tau}{2}\right)\sin\left(2\pi\nu_1\frac{\tau}{2}\right)} \right) - 2\pi\nu_1 \tag{S22}$$

$$a_{\perp} = \sqrt{(2\pi\nu_2)^2 - \left(2\pi\nu_1 + a_{||}\right)^2} \tag{S23}$$

These values are reported in the third column of Table I.

3. *Error calculation*

The fitting was done in Matlab using the Levenberg-Marquardt algorithm. Reported uncertainties in $\nu_{1..3}$ were computed using linearization of the model functions and were cross validated using bootstrapping. The uncertainties in NMR constants were calculated using standard error propagation.

Linearization allows us to construct confidence intervals from estimating the covariance matrix as in the case of linear regression [S2]. Denoting the estimator of our model parameters by $\hat{\beta}$, the estimated covariance matrix of $\hat{\beta}$ is

$$\Sigma = \left(J^T(\hat{\beta})J(\hat{\beta})\right)^{-1}\hat{\sigma}^2_{\text{res}}, \tag{S24}$$

where $J(\hat{\beta})$ is the Jacobian matrix of the model function as used in the Levenberg-Marquardt algorithm and $\hat{\sigma}^2_{\text{res}}$ is the estimated sample variance of the residuals with (n-p) degrees of freedom. The estimator of the standard deviation of the j-th model parameter is

$$\sigma_\nu = \sqrt{\hat{\text{var}}(\hat{\beta}_j)} = \sqrt{\Sigma_{jj}\hat{\sigma}^2}, \tag{S25}$$

where Σ_{jj} denotes the j-th diagonal element of the covariance matrix.

The bootstrapping was done by fitting our data 3000 times with additional noise and calculating the standard deviation of the fit results. The added noise was generated once by resampling residuals with replacement and a second time by generating normal distributed random numbers with variance $\hat{\sigma}^2_{\text{res}}$ estimated from the residuals. Bootstrapping produced in all case slightly smaller standard deviations. Therefore, we used the standard deviations derived from the Jacobian to quantify the uncertainty of the measured frequencies ν_i.

For illustration purposes, we compare our best fit with two fits having a ($\pm 2\sigma$) frequency deviation from our claimed signal frequency for the data set shown in Fig. S2 (b), see Fig. S3. We plot the residuals as function of time and in a histogram for each case. In the time plot, one can see that the residuals are oscillating for the two control fits ($\nu = \nu_3 \pm 2\sigma_{\nu_3}$ fixed). Furthermore, the control fits show an increased spread of the residuals in the histograms.

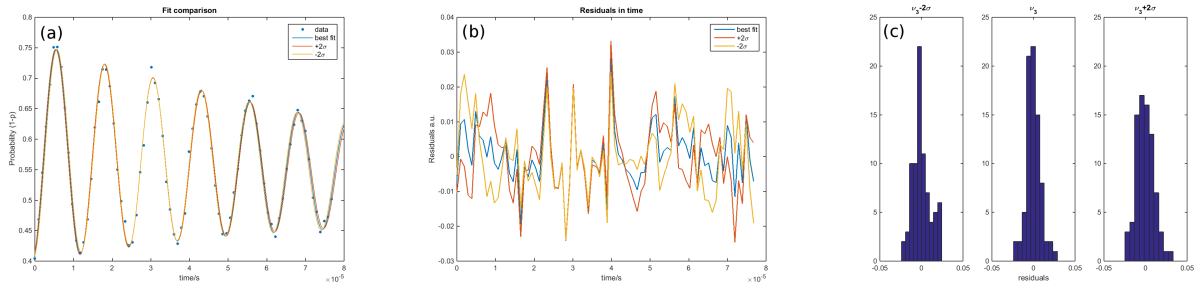

FIG. S3: Plots illustrating the sensitivity of the fit to small frequency shifts. (a) Comparison between best fit and fits with a fixed frequency that is deviating from the best fit by $\pm 2\sigma_{\nu_3}$. (b) Residuals of fits plotted in time. Oscillations are seen for the fits with $\pm 2\sigma_{\nu_3}$, showing that ν_3 indeed is a best fit. (c) Histograms of residuals. An increased spread is seen for the fits with $\pm 2\sigma_{\nu_3}$.

IV. ESTIMATION OF ^{13}C POSITIONS

A. Calculation of angle θ and distance r from $a_{||}$ and $a_{\perp}$

Assuming that the hyperfine interaction is dipolar, we can determine the distance r and internuclear angle θ between the NV center and the ^{13}C from hyperfine constants $a_{||}$ and $a_{\perp}$:

$$a_{||} = \frac{\mu_0 \gamma_e \gamma_n \hbar}{4\pi r^3}(3\cos^2\theta - 1), \tag{S26}$$

$$a_{\perp} = \frac{\mu_0 \gamma_e \gamma_n \hbar}{4\pi r^3} 3\cos\theta \sin\theta. \tag{S27}$$

$a_{||}$ and $a_{\perp}$ have units of angular frequency. The angle θ and distance r as a function of $a_{||}$ and $a_{\perp}$ are:

$$\theta = \arctan\left\{\frac{1}{2}\left(-3\frac{a_{||}}{a_{\perp}} + \sqrt{9\frac{a_{||}^2}{a_{\perp}^2} + 8}\right)\right\}, \tag{S28}$$

$$r = \left\{\frac{\mu_0 \gamma_e \gamma_n \hbar (3\cos^2\theta - 1)}{4\pi a_{||}}\right\}^{1/3}. \tag{S29}$$

Comparing our results to Smeltzer et al. [S3] we find best agreement with the ^{13}C sites E and F, which are about 3 Å away from the vacancy site of the NV center. For these ^{13}C sites the hyperfine constants have, however, a significant contribution of the Fermi contact interaction. According to *ab initio* values by Gali et al., Ref. [S4], the Fermi contact term ranges from about 2.2 MHz to 4.3 MHz for the different ^{13}C sites. We have calculated the expected internuclear distance and angle for the three sites given in Ref. [S4], and collected the results in Table II. The values were obtained by subtracting the contact hyperfine coupling a_{iso} from $a_{||}$ and then calculating r and θ according

to Eqs. (S28) and (S29). These values are approximate at best, however, because the a_{iso} has an error of several 100 kHz resulting in a large error in θ.

R_{vac}	2.90 Å	2.92 Å	2.93 Å
$a_{\mathrm{iso}}/2\pi$	3.6 MHz	2.2 MHz	4.3 MHz
r	3.7 Å	2.8 Å	3.4 Å
θ	32°	11°	70°

TABLE II: ^{13}C site distance r and polar angle θ calculated for our measured hyperfine constants $a_{||}$ and $a_{\perp}$ assuming different contributions from the Fermi contact interaction. Fermi contact term was taken from Table 2 in Ref. [S4].

B. Influence of magnetic field misalignment

Measurements were done at magnetic field strengths between 170 mT and 200 mT. The magnetic field was aligned along the NV symmetry axis (the diamond (111) axis or ZFS axis) to within about 2° or better, in order to achieve good ODMR contrast.

Since the internuclear angle θ is measured against the direction of the external bias field, misalignment of the external field directly leads to an error in the angle inferred from the measurement. In this section we briefly discuss how a small field misalignment impacts $a_{||}$ and $a_{\perp}$.

1. *Change in spatial angle*

Fig. S4 shows a schematic of the effective magnetic field B_{eff} felt by the NV center (for its $m_s = -1$ state) when the bias field B_0 is misaligned by an angle γ from the symmetry axis. Depending on the magnitude and direction of the applied external magnetic field B_0, the effective misalignment angle ϵ can be larger or smaller than γ,

$$\sin(\epsilon) = \frac{B_{\mathrm{ZFS}} \sin(\gamma)}{\sqrt{B_0^2 + B_{\mathrm{ZFS}}^2 - 2B_0 B_{\mathrm{ZFS}} \cos(\gamma)}}, \tag{S30}$$

where $B_{\mathrm{ZFS}} = D/\gamma_e$ is the magnetic field felt by the NV center due to the zero-field splitting $D = 2\pi \times 2.87\,\mathrm{GHz}$ and $\gamma_e = 2\pi \times 28\,\mathrm{GHz/T}$ is the electron gyromagnetic ratio. In our case, the

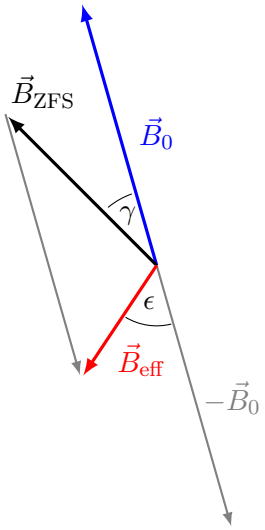

FIG. S4: Schematic depicting the effective B_{eff} field in the case of a misaligned external B_0 field with respect to the [111] crystallographic axis of the diamond.

external field was about twice the zero field splitting, leading to an effective misalignment angle of about $\epsilon \cong 2\gamma$.

2. *Change in the angle between the electronic and nuclear magnetization vectors*

The difference between the two angles γ and ϵ lead also to another effect. As the ^{13}C nuclear spin is aligned with the external magnetic field B_0 (misalignment γ) while the NV electronic spin is aligned with the effective field B_{eff} (misalignment ϵ), the two spins will have a different quantization axes. For simplicity, we will assume that the external magnetic field is tilted in the zx-plane. In that case, the Hamiltonian as presented in Eq. S5 changes to

$$\hat{H}_{\mathrm{free}} = \omega_0 \hat{I}_{\tilde{z}} + a_{||} \hat{S}_z \hat{I}_z + a_{\perp} \hat{S}_z \hat{I}_x, \tag{S31}$$

where the $(\tilde{x}, \tilde{z})$ coordinate system is aligned with the quantization axis of the ^{13}C nuclear spin. To find $\tilde{a}_{||}$ and $\tilde{a}_{\perp}$ we transform all nuclear spin operators, where

$$\hat{I}_z = \cos(\gamma - \epsilon)\hat{I}_{\tilde{z}} + \sin(\gamma - \epsilon)\hat{I}_{\tilde{x}} \tag{S32}$$

$$\hat{I}_x = \cos(\gamma - \epsilon)\hat{I}_{\tilde{x}} - \sin(\gamma - \epsilon)\hat{I}_{\tilde{z}}. \tag{S33}$$

This gives us

$$\hat{H}_{\mathrm{free}} = \omega_0 \hat{I}_{\tilde{z}} + \underbrace{\left(a_{||}\cos(\gamma-\epsilon) - a_{\perp}\sin(\gamma-\epsilon)\right)}_{\tilde{a}_{||}} \hat{S}_z \hat{I}_{\tilde{z}} + \underbrace{\left(a_{\perp}\cos(\gamma-\epsilon) + a_{||}\sin(\gamma-\epsilon)\right)}_{\tilde{a}_{\perp}} \hat{S}_z \hat{I}_{\tilde{x}}. \tag{S34}$$

Assuming $\gamma - \epsilon = 2^\circ$ we get $a_{||}(\cos(\gamma - \epsilon) - 1) = 2.5$ kHz and $a_\perp \sin(\gamma - \epsilon) = 18$ kHz for the ^{13}C of Table I. Thus, even a small misalignment has a significant impact on $a_{||}$ and $a_\perp$ which can easily be larger than the uncertainty of the measurement scheme. This has two consequences: One the one hand, a very precise alignment of the external bias field is required to obtain reproducible values of $a_{||}$ and $a_\perp$. On the other hand, a deliberate misalignment of the bias field may be used to discriminate between contact and dipolar hyperfine coupling contributions, or to estimate the third (azimuthe) angle of the ^{13}C spatial position.

[S1] T. H. Taminiau, J. J. T. Wagenaar, T. V. der Sar, F. Jelezko, V. V. Dobrovitski, and R. Hanson, Phys. Rev. Lett. **109**, 137602 (2012).

[S2] G. A. F. Seber and C. J. Wild, *Statistical Inference* (John Wiley & Sons, Inc., 2005), pp. 191–269, ISBN 9780471725312, URL http://dx.doi.org/10.1002/0471725315.ch5.

[S3] B. Smeltzer, L. Childress, and A. Gali, New Journal of Physics **13**, 025021 (2011), URL http://stacks.iop.org/1367-2630/13/i=2/a=025021.

[S4] A. Gali, M. Fyta, and E. Kaxiras, Phys. Rev. B **77**, 155206 (2008).